Multicritical phase diagram of the electronic states in $Sm_{1-x}Sr_xMnO_3$ ($0.3<x<0.6$) single crystals with controlled carrier density

Y. Tomioka,[1] H. Hiraka,[2] Y. Endoh,[2] and Y. Tokura[1,3,4]

[1]*Correlated Electron Research Center (CERC), National Institute of Advanced Industrial Science and Technology (AIST), Tsukuba 305-8562, Japan*

[2]*Institute of Material Research (IMR), Tohoku University, Katahira, Sendai 980-8577, Japan*

[3]*Spin Superstructure Project, ERATO, Japan Science and Technology Corporation (JST), Tsukuba 305-8562, Japan*

[4]*Department of Applied Physics, University of Tokyo, Tokyo 113-8656, Japan*

(Received 21 February 2006; revised manuscript received 18 July 2006; published 27 September 2006)

For $Sm_{1-x}Sr_xMnO_3$ ($0.3<x<0.6$) single crystals, the x-dependent magnetic as well as transport properties, including the field-induced insulator-to-metal transition, have been studied. The ferromagnetic metal at $x<0.5$ changes to the layered (A-type) antiferromagnetic nonmetal at $x>0.5$. At $x\sim0.5$ furthermore, where both T_C and T_N become comparable, the charge or orbital ordering appears. At $x=0.50$, the crystal first undergoes the transition to the layered-antiferromagnetic state at $\sim$130 K and subsequently to the CE-type antiferromagnetic charge or orbital-ordered state at $\sim$80 K as temperature decreases. The coexisting correlations of the charge or orbital ordering, ferromagnetic and layered-antiferromagnetic orderings are observed to evolve toward the tricritical point from high temperature around $x=0.5$. The magnetic-field induced metal-insulator phenomena have also been studied for the $x=0.49$, 0.50, and 0.51 crystals, and we have demonstrated on the temperature versus magnetic-field plane the competing features among the charge or orbital-ordered insulator, the layered (A-type) antiferromagnetic nonmetal, and the ferromagnetic metal.

DOI: 10.1103/PhysRevB.74.104420 PACS number(s): 71.27.+a, 71.30.+h, 75.30.Kz

I. INTRODUCTION

For recent years, the manganese oxides with perovskite or layered-perovskite structure have extensively been studied, since the materials show a lot of intriguing phenomena such as colossal magnetoresistance (CMR) and insulator-metal transitions induced by various external stimuli.[1] In $RE_{1-x}AE_xMnO_3$ (RE and AE being rare-earth and alkaline-earth elements, respectively), a decrease in the averaged ionic radius of the RE^{3+} and AE^{2+} cations [$r_A=(1-x)r_{RE3+}+xr_{AE2+}$] leads to an increase in the tilting of MnO_6 octahedra in terms of the lattice distortion of the perovskite structure, and thus a decrease in the effective one-electron bandwidth of the e_g band (W).[2] In the narrowed W case, the competing interactions against the double exchange (DE)[3–5] interaction become important, e.g., the collective Jahn-Teller distortion, the antiferromagnetic interaction between local t_{2g} spins, the charge or orbital ordering (CO/OO), and so forth. In $RE_{1-x}Sr_xMnO_3$, the ferromagnetic metal (FM) due to DE is most stabilized for RE=La, and the T_C becomes as high as 370 K at $x\sim0.35$.[6,7] For RE=Nd, the W of which is reduced, the FM appears at $0.3<x<0.5$ with the optimal $T_C\sim280$ K at $x=0.4$, and the CO/OO appears in the vicinity of $x=0.5$ ($0.48<x<0.52$).[8–10] Subsequently, the A-type (layered) and the C-type (chainlike) antiferromagnetic states appear at $0.5<x<0.6$ and $x>0.6$, respectively. The variation of the ground state with x[8–10] is in good agreement with the theoretical calculation.[11,12]

As a further step to the reduction of W, the phase diagrams for RE=Sm have been reported on the polycrystalline[13] and single crystal.[14,15] The optimal T_C is further decreased to about 130 K, which is at $x\sim0.45$.[13–15] According to Ref. 13, the ground states are the FM at $0.3<x\leqslant0.52$, and the antiferromagnetic insulating phase for $x>0.52$, respectively. For $0.4\leqslant x\leqslant0.6$, the charge ordering occurs and the critical temperature (T_{CO}) increases from $\sim$140 to 205 K with an increase in x, which was confirmed by the electron diffraction measurement.[13] The CMR is seen for $0.3\leqslant x\leqslant0.52$.[16] In Refs. 14 and 15 it has been indicated that a sharp boundary between a ferromagnetic and an antiferromagnetic phase exists at $x\sim0.5$, and that a local charge-ordering phase appears for $0.5<x<0.575$. Besides the studies on the x-dependent phase diagrams, structural investigations on the $^{154}Sm_{0.5}Sr_{0.5}MnO_3$ (Ref. 17) and a change of the ground state near $x=0.5$ upon the oxygen isotope substitution[18–21] have been reported. In the light of the possible phase separation,[22–26] an increased quenched disorder arising from the substitution of RE with AE should also be taken into account for such a narrowed W system as RE=Sm.[27–29] Here, the magnitude of quenched disorder can be quantified by the variance of the ionic radii, $\sigma^2=\Sigma(xr_i^2-r_A^2)$, where x_i and r_i are the fractional occupancies and the effective ionic radii of cations of RE and AE, respectively.[27,28] In this paper, we describe the critically x-dependent properties of $Sm_{1-x}Sr_xMnO_3$ ($0.3<x<0.6$) single crystals as the representative materials for the multicritical phase competition. In the vicinity of $x=0.5$, a change in x by one percent dramatically modifies the ground state, and the three different phases are clearly identified as a function of x, a ferromagnetic metal ($x\leqslant0.48$), a charge or orbital-ordered insulator (CO/OOI) ($x=0.49$ and 0.5), and an A-type (layered) antiferromagnetic nonmetal ($x\geqslant0.51$). As a result, the CO/OOI appears only at $x=0.49$ and 0.5, and the coexistence of two phases is only seen at $x=0.49$ (FM and CO/OOI). Furthermore, it is found from the measurement of an x-ray diffuse scattering that for $x=0.48$ and 0.51 a short-range CO/OO exists (disappears) above (below) T_C and T_N, respectively. In $Sm_{1-x}Sr_xMnO_3$ single crystals, therefore, the

competition among the FM, CO/OO and the *A*-type antiferromagnetic nonmetal becomes prevailing in the vicinity of $x=0.5$, and the tricritical feature is revealed in the *x*-dependent electronic phase diagram. As for the format of this paper, in Sec. II we first describe experimental procedures. Subsequently in Sec. III, we present an overview of the electronic phase diagram (III A), and an insulator-to-metal transition in magnetic fields (III B). The summary is given in Sec. IV.

II. EXPERIMENTAL PROCEDURES

Single crystals of $Sm_{1-x}Sr_xMnO_3$ ($0.3<x<0.6$) were prepared by the floating zone method. The mixed powders of Sm_2O_3, $SrCO_3$, and Mn_3O_4 with a prescribed ratio were first calcined at 1050–1100 °C for 12–24 hours in air. The specimens were pulverized and again sintered in the same condition. Then, the powders were pressed into a rod with ~4 mm in diameter and ~50 mm in length. The rod was fired at 1300–1400 °C for 12–24 hours in air. The crystal growth was performed in an oxygen atmosphere with rotating feed and seed rods in opposite directions. The growth rate was set at 10–20 mm/h. Rietveld refinement of the powder x-ray diffraction pattern indicated that the obtained crystal is of a single phase, and that the crystal structure is orthorhombic *Pbnm* ($a_0 \sim b_0 \sim c_0/\sqrt{2} \sim \sqrt{2}a_p$, where a_p is the lattice parameter of the pseudocubic lattice). The cation ratio of the obtained crystals was also checked by the inductively coupled plasma (ICP) spectroscopy. The analyzed cation ratio, the lattice parameters, and the transition temperatures for several crystals of $Sm_{1-x}Sr_xMnO_3$ are listed in Table I. Magnetization was measured by a SQUID magnetometer (MPMS, Quantum Design Inc.). Resistivity in magnetic fields was measured in a cryostat equipped with a superconducting magnet up to 9 T. The electrodes for the resistivity measurement were made by gold or silver paste.

For several crystals, a single crystal x-ray diffraction was performed, using an imaging plate system monochromated with Mo $K\alpha$ radiation. A crystal was mounted on a goniometer with a (0 0 1) plane of the pseudocubic setting almost perpendicular to a beam axis. The temperature was changed down to ~50 K with the use of a closed cycle helium refrigerator. In addition, the experimental detail about the inelastic neutron scattering study on the $^{154}Sm_{0.55}Sr_{0.45}MnO_3$ crystal has been described in Ref. 30.

III. RESULTS AND DISCUSSION

A. An overview of the electronic phase diagram

Figure 1 shows the electronic phase diagram for $Sm_{1-x}Sr_xMnO_3$ ($0.3<x<0.6$) crystals. For $x<0.5$, the ferromagnetic metal dominates, and the T_C becomes maximal (~135 K) at $x \sim 0.45$, which is in agreement with the results in Refs. 13–15. For $x>0.5$, similarly to the systems of $RE_{1-x}Sr_xMnO_3$ with *RE*=La, Pr, and Nd, the antiferromagnetic state [perhaps *A*-type with the ordering of (x^2-y^2) orbital] becomes prevailing, and the T_N increases with an increase in *x*. At $x \sim 0.5$, where both T_C and T_N become comparable, the CO/OOI appears, but in spite of that T_{CO} is decreased to about 100 K. In Fig. 1, therefore, the point of ($x \sim 0.5, T \sim 120$ K) is considered as the multicritical point, near which the three phases, FM, CO/OOI, and the *A*-type antiferromagnetic state, are competing with each other.

TABLE I. The analyzed cation ratio, lattice parameters, and transition temperatures of $Sm_{1-x}Sr_xMnO_3$ prepared by the floating zone method ($0.4 \leqslant x \leqslant 0.55$).

x (Nominal)	*x* Sr/(Sm+Sr)[a]	Lattice parameters, a_0, b_0, and c_0 [Å]	T_C,[b] T_{CO},[c] and T_N[d] [K]
0.40	0.398	$a_0=5.4412$, $b_0=5.4334$, $c_0=7.6836$	[b]122.9
0.45	0.451	$a_0=5.4404$, $b_0=5.4297$, $c_0=7.6593$	[b]134.8
0.48	0.480	$a_0=5.4431$, $b_0=5.4210$, $c_0=7.6442$	[b]129.0
0.49	0.493	$a_0=5.4449$, $b_0=5.4202$, $c_0=7.6411$	[d]116.5, [c]118.3
0.50	0.502	$a_0=5.4453$, $b_0=5.4184$, $c_0=7.6339$	[c]99.7, [d]128.0
0.51	0.510	$a_0=5.4463$, $b_0=5.4171$, $c_0=7.6285$	[d]142.5
0.55	0.548	$a_0=5.4651$, $b_0=5.4277$, $c_0=7.6167$	[d]178.5

[a]The cation ratio has been determined by the ICP spectroscopy.
[b]The averaged value determined from the resistivity in the cooling and warming runs.
[c]The averaged value determined from the resistivity in the cooling and warming runs.
[d]The averaged value determined from the resistivity in the cooling and warming runs.

In Fig. 2 are shown the temperature profiles of magnetization [(a), (e)], the resistivity [(b), (f)], the lattice param-

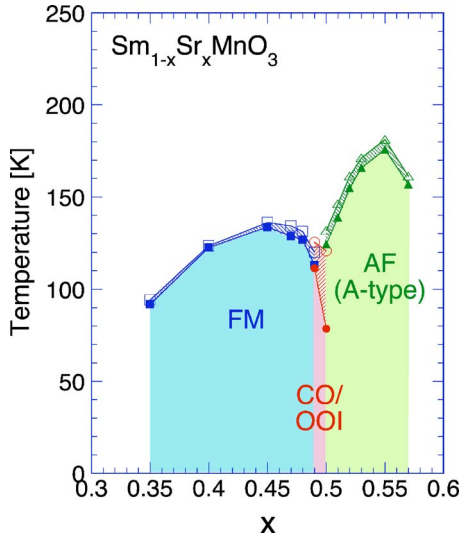

FIG. 1. (Color online) The electronic phase diagram of $Sm_{1-x}Sr_xMnO_3$ ($0.3<x<0.6$). The ferromagnetic metal, the *A*-type antiferromagnetic state and the charge/orbital-ordered insulator are denoted as FM, AF (*A*-type) and CO/OOI, respectively. The transition temperatures from (to) the FM, AF, and CO/OOI are denoted as open (closed) squares, triangles, and circles, respectively.

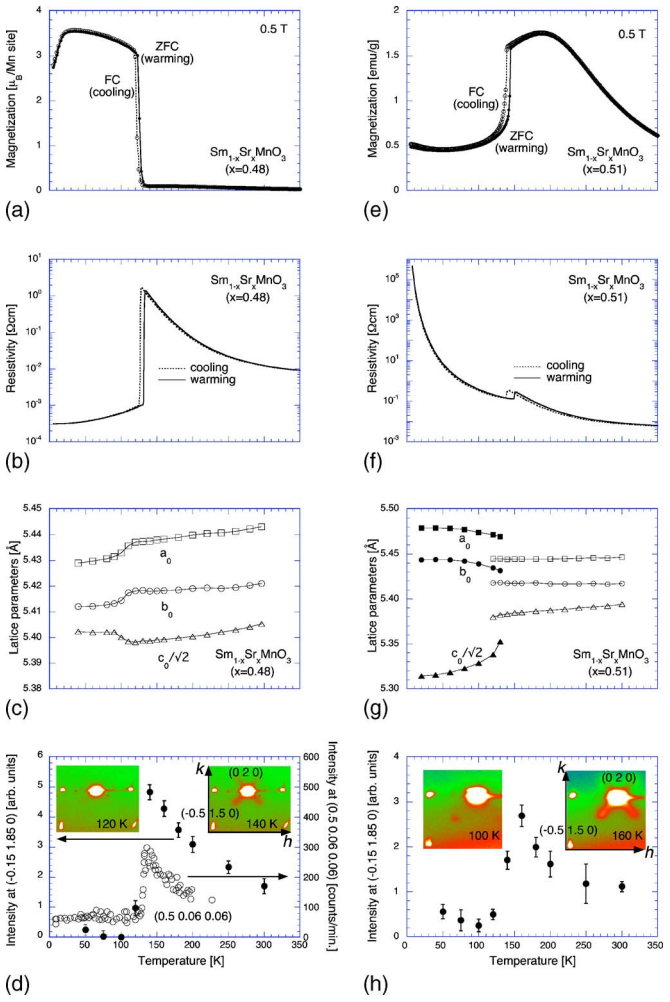

FIG. 2. (Color online) The temperature profiles of magnetization [(a) and (e)], resistivity [(b) and (f)], lattice parameters [(c) and (g)], and the intensity of x-ray diffuse scattering around (0 2 0) [(d) and (h)] for the $x=0.48$ (a)–(d) and 0.51 (e)–(h) crystals, respectively. In Fig. 2(d), the temperature profiles of the antiferromagnetic neutron diffuse scattering, (0.5 0.06 0.06) for the $^{154}Sm_{1-x}Sr_xMnO_3$ ($x=0.45$) single crystal are also shown (cited from Ref. 30. Insets show the x-ray diffuse scatterings at 120 K, 140 K for $x=0.48$ (d), and 100 K, 160 K for $x=0.51$ (h), respectively. The reflections are indexed in the pseudocubic setting. The reflections at both the left and right sides of (0 2 0) are due to the twinning of the crystal.

eters [(c), (g)], and the intensity of x-ray diffuse scattering around (0 2 0) diffraction in the pseudocubic indices [(d), (h)][31] for the $x=0.48$ (left) and 0.51 (right) crystals, respectively. In Figs. 2(d) and 2(h), the intensity of the diffuse scattering at (−0.15 1.85 0) was estimated by fitting the profile of $(-0.15+\delta\ 1.85+\delta\ 0)$ $(-0.25\leqslant\delta\leqslant 0.25)$ with a Gaussian form, and normalized by an intensity of (1 1 0) diffraction. [This estimation in the pseudocubic indices corresponds to that of the intensity of the diffuse scattering around (2 2 0) by fitting the profile of $(1.7\ 2+\Delta h\ 0)$ $(-0.5\leqslant\Delta h\leqslant 0.5)$ in the orthorhombic *Pbnm* $(a_0\sim b_0\sim c_0/\sqrt{2})$ indices.][31] The charge or orbital correlation in a short range is well quantified by an intensity of the diffuse scattering.[32,33]

As shown in Figs. 2(a) and 2(b), the $x=0.48$ crystal undergoes the transition to the FM at ∼130 K. The transition is accompanied by the slight elongation of c_0, as well as contractions of a_0 and b_0 as shown in Fig. 2(c). In accord with this, the intensity of the x-ray diffuse scattering marked with closed circles is distinctly suppressed below ∼130 K [Fig. 2(d)]. These changes of the structural properties indicate that for the $x=0.48$ crystal the CO/OO correlation is enhanced, while remaining short range as the temperature approaches T_C, but it is suddenly removed at T_C.[31]

In Fig. 2(d) with the right ordinate we show the temperature evolution of the antiferromagnetic neutron diffuse scattering at (0.5 0.06 0.06) for the $^{154}Sm_{1-x}Sr_xMnO_3$ ($x=0.45$) single crystal ($T_C=134.8$ K),[30] by which the magnitude of the *A*-type antiferromagnetic correlation in a short range may be well quantified. Since the temperature evolutions of the physical quantities (magnetization, resistivity, lattice parameters, and x-ray diffuse scattering) for the $x=0.48$ crystal as shown in Figs. 2(a)–2(c) are almost identical with those for the $x=0.45$ crystal,[30] the *A*-type antiferromagnetic interaction is likely to be present with a comparable magnitude also in the $x=0.48$ crystal. Although the *A*-type antiferromagnetic state does not appear as the ground state for $x<0.5$, Fig. 2 (left) indicates that even for $x<0.5$ the *A*-type antiferromagnetic correlation in a short range may exist at $T>T_C$ in addition to the CO/OO correlation in a short range. The observation of both the CO/OO correlation with staggered $(3x^2-r^2)/(3y^2-r^2)$ orbital states and the orbital or spin fluctuation with (x^2-y^2) orbital and *A*-type spin correlation indicates the presence of the multicritical point around $x=0.5$ and 120 K (see Fig. 1).

As shown in Figs. 2(e) and 2(f), both the magnetization and resistivity show decreasing at ∼140 K, indicating that the $x=0.51$ crystal undergoes the transition to the (*A*-type) antiferromagnetic and nonmetallic state at ∼140 K. In Fig. 2(g), the contraction of c_0 and the elongations of a_0 and b_0 are seen at the same temperature. Upon the transition to the *A*-type antiferromagnetic state, such a structural change is expected due to the ordering of the (x^2-y^2) orbital within the *ab* plane of the orthorhombic *Pbnm* crystal lattice.[34] In Fig. 2(h), the intensity of x-ray diffuse scattering, i.e., the CO/OO in a short range is observed to be weakened below ∼140 K. Thus, the ground state of the $x=0.51$ crystal is the *A*-type antiferromagnetic nonmetallic state.

Next, we further blow up the *x*-dependent properties in the $Sm_{1-x}Sr_xMnO_3$. In Fig. 3 are shown temperature profiles of the magnetization [(a), (e)], the resistivity [(b), (f)], the lattice parameters [(c), (g)], and the intensity of x-ray diffuse scattering [(d), (h)] for the $x=0.49$ and 0.50 crystals, respectively. For $x=0.50$, as shown in Figs. 3(e) and 3(f), the magnetization and resistivity show a decrease around 130 K, which is similar to the transition at ∼140 K for the $x=0.51$ crystal [Figs. 2(e) and 2(f)]. With a further decrease in temperature, however, another transition is seen around 80 K in the cooling process, accompanied by a decrease in magnetization and an increase in resistivity. The transition in the warming process occurs around 120 K, showing an appreciable thermal hysteresis. In Fig. 3(g), the contraction of c_0, as well as the elongations of a_0 and b_0, are seen at ∼120 K. In Fig. 3(h), the magnitude of the diffuse scattering around (0 2 0) as a CO/OO correlation in a short range increases as the

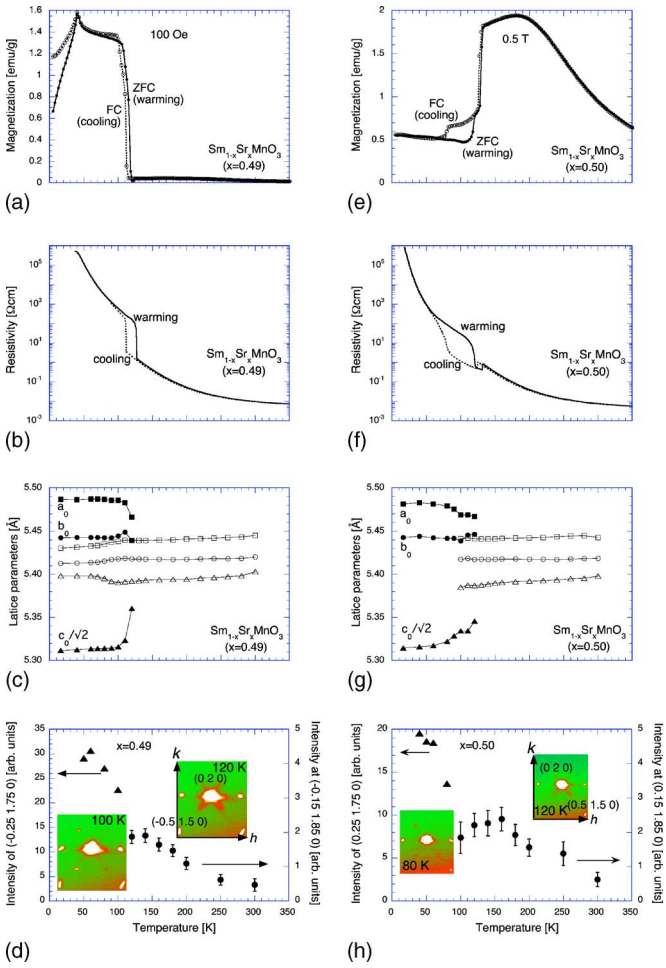

FIG. 3. (Color online) The temperature profiles of magnetization [(a) and (e)], resistivity [(b) and (f)], lattice parameters [(c) and (g)], and the intensity of x-ray diffuse scattering around (0 2 0), as well as the peak intensity of the superlattice diffraction of (±0.25 1.75 0) [(d) and (h)] for the $x=0.49$ (a)–(d) and 0.50 (e)–(h) crystals, respectively. In Figs. 3(d) and 3(h), the estimation of the intensity of the diffuse scattering is the same as that in Figs. 2(d) and 2(h). Insets show the diffuse scatterings at 100 K, 120 K for $x=0.49$ (d), and 80 K, 120 K for $x=0.50$ (h), respectively. The reflections are indexed in the pseudocubic setting. The reflections at both the left and right sides of (0 2 0) are due to the twinning of the crystal.

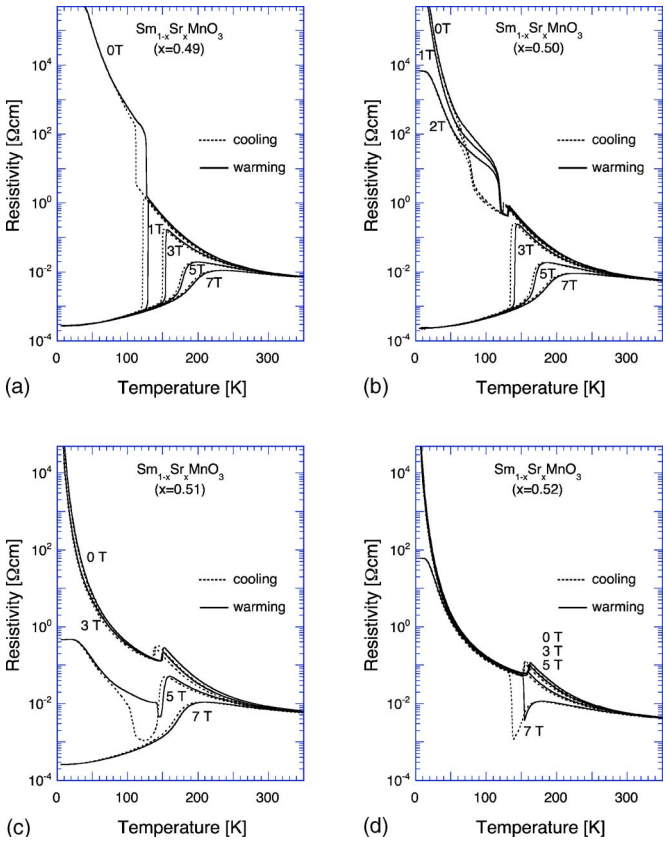

FIG. 4. (Color online) The temperature profiles of resistivity in magnetic fields for the $Sm_{1-x}Sr_xMnO_3$ crystals with $x=0.49$ (a), 0.5 (b), 0.51 (c), and 0.52 (d), respectively. The cooling and warming runs are denoted as dotted and solid lines, respectively.

temperature decreases from 300 to 160 K. Below 80 K, however, the diffuse scattering disappears but the distinct superlattice diffraction of (1/4 7/4 0) is observed as the indication of CO/OO in a long range. Thus, with a lowering temperature, the $x=0.5$ crystal first undergoes the transition to the *A*-type antiferromagnetic state and successively to the *CE*-type antiferromagnetic CO/OO state.

In the case of $x=0.49$, as shown in Fig. 3(a), a transition to the ferromagnetic state seems to take place at ~110 K. In Fig. 3(b), in contradiction with the ferromagnetic transition, the resistivity shows a steep increase (decrease) at ~110 K (~125 K) in the cooling (warming) run, which rather suggests the first-order transition to (from) the CO/OO. The temperature profiles of powder x-ray diffraction pattern in Fig. 3(c) indicate that the two phases are coexisting below ~120 K. For one phase (open squares, circles, and triangles), the a_0 and b_0 contract while c_0 elongates upon the transition, which is similar to the case of the $x=0.48$ crystal. For another phase (closed squares, circles, and triangles), they are vice versa. In Fig. 3(d), the magnitude of the diffuse scattering around (0 2 0) increases as the temperature decreases from 300 to 140 K. Below 100 K, however, the diffuse scattering disappears but the superlattice diffraction of (−1/4 7/4 0) is discerned. Thus, for the $x=0.49$ crystal the FM and CO/OOI are coexisting below ~110 K.[17] The resistivity of the $x=0.49$ crystal still keeps insulating at low temperature as shown in Fig. 3(b), however, the ratio of the FM in the crystal is considered to be less than the percolation limit. According to the observed magnetization value ($0.05\mu_B$/Mn site at 100 Oe) compared with the ideal saturation value ($3.5\mu_B$/Mn site), the volume fraction of the FM of the crystal is estimated to be less than 1.5%. The important feature to be noticed here is that the transition temperatures (~110 K) to the ferromagnetic state and to the CO/OO state, which coexist in the $x=0.49$ crystal, are almost identical. This is a hallmark of the multicritical phase competition.

B. An insulator to metal transition in magnetic fields

To argue the phase stability against magnetic field we show in Figs. 4(a)–4(d) the temperature profiles of resistivity in magnetic fields for the crystals of $x=0.49$–0.52, respec-

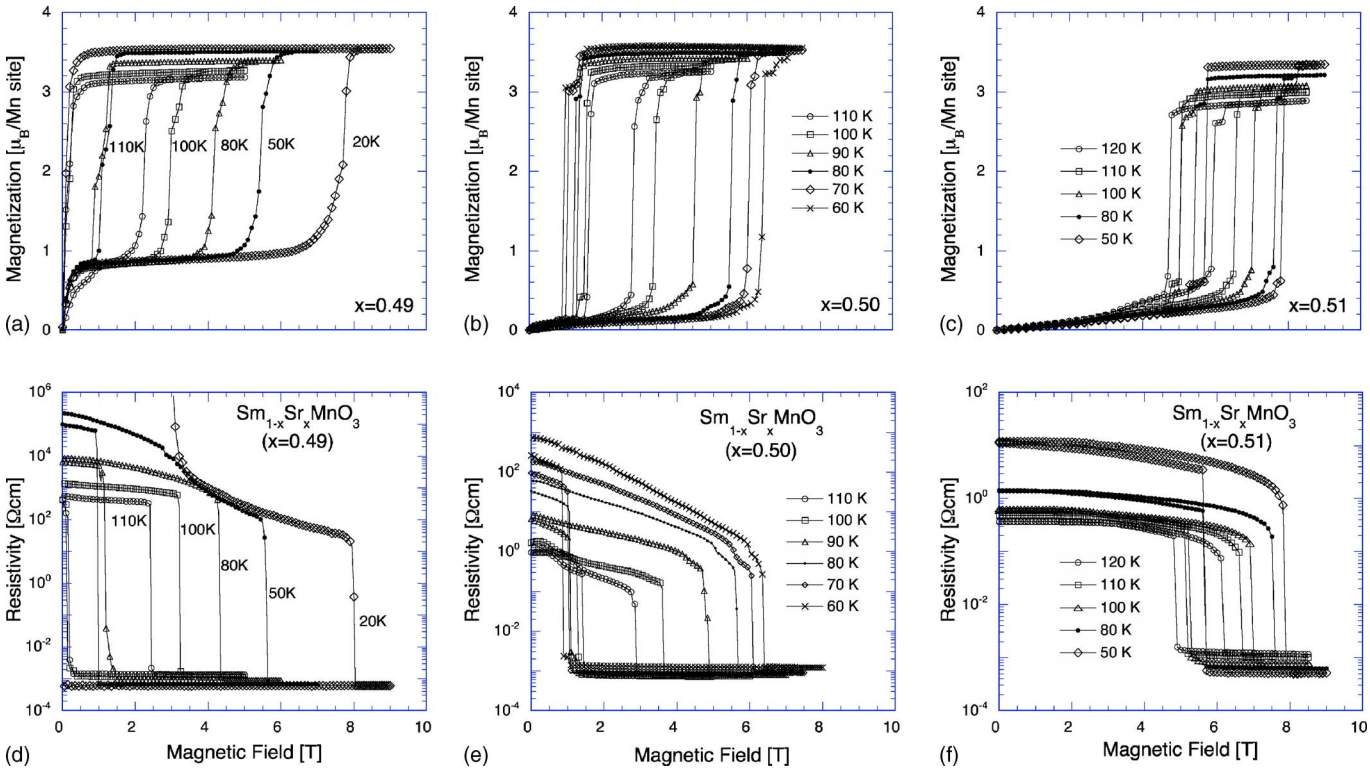

FIG. 5. (Color online) The magnetization (a)–(c) and resistivity (d)–(f) isotherms for the $Sm_{1-x}Sr_xMnO_3$ crystals with $x=0.49$ [(a) and (d)], 0.5 [(b) and (e)], and 0.51 [(c) and (f)], respectively.

tively. In Figs. 4(a) and 4(b), the CO/OOI as the ground state changes to the FM at $\mu_0 H \geqslant 1$ T for $x=0.49$ and at $\mu_0 H \geqslant 3$ T for $x=0.5$, respectively. For $x=0.51$, as shown in Fig. 4(c), the *A*-type antiferromagnetic state remains up to 3 T, while it turns into a FM at 7 T. At 5 T, a metallic state is seen between ~130 and ~110 K in the cooling run, but it changes to an *A*-type antiferromagnetic state (perhaps with canting) below ~100 K. In the warming run, the canting remains up to ~150 K. For $x=0.52$, as shown in Fig. 4(d), the *A*-type antiferromagnetic state is more stabilized and subsists to 5 T although a negative magnetoresistance is seen above T_N due to the field-enhanced ferromagnetic correlation. At 7 T, however, a metallic state is induced between ~170 and ~140 K (~160 and 170 K), but it is replaced with the *A*-type antiferromagnetic state below ~130 K (~150 K) in the cooling (warming) run. In the case of $x=0.52$, the *A*-type antiferromagnetic state survives at low temperatures even at 7 T.

Figure 5 shows the magnetization (a)–(c) and resistivity (d)–(f) isotherms for the $x=0.49$, 0.5, and 0.51 crystals, respectively. All the crystals show the metamagnetic transitions at some critical magnetic fields, which are accompanied by the steep changes in resistivity. For $x=0.49$, as an example, the magnetization at 50 K shows the metamagnetic transition at ~5.5 and ~1 T in the field-increasing and -decreasing runs, respectively. Accordingly, the resistivity at the same temperature shows the steep decrease and increase in the corresponding magnetic fields. It is noted in Fig. 5(a), however, that a magnetization by $\sim 0.8 \mu_B$/Mn site is already seen at low fields ($\mu_0 H < 1$ T), which is ascribed to the coexistence of the FM with the CO/OOI for $x=0.49$ as indicated in Figs. 3(a)–3(d).

Figure 6 shows the phase diagrams plotted on the temperature versus the magnetic-field plane which are composed of the CO/OOI, the *A*-type antiferromagnetic nonmetal, and the FM for the $x=0.49$, 50, and 0.51 crystals. In the case of $x=0.49$, the CO/OOI changes to the FM by application of an external magnetic field, although a small amount of FM already exists in the CO/OOI. In the case of $x=0.50$, as indicated in Fig. 3, the transition above ~80 K is considered between the *A*-type antiferromagnetic nonmetal and the FM, while that below ~80 K is between the CO/OOI and FM. Finally, in the case of $x=0.51$, the transition is between the *A*-type antiferromagnetic nonmetal and the FM. It is noted in Fig. 6 that the widths of the hystereses at low temperatures in the phase diagrams for $x=0.49$ and 0.5, which is related to the transition between the CO/OOI and the FM, are rather pronounced as compared with those for $x=0.51$ between the *A*-type antiferromagnetic nonmetal and the FM.

The present phase diagrams reveal the two routes to the magnetic-field-induced nonmetal-to-metal transition, that is via the competition between the *A*-type antiferromagnetic state and the FM, in addition to the already well-addressed one between the CO/OOI and the FM, near such a multicritical region.

IV. SUMMARY

We have studied the *x*-dependent properties of the $Sm_{1-x}Sr_xMnO_3$ ($0.3 < x < 0.6$) single crystals. The ferromagnetic metal at $x<0.5$ changes to the *A*-type antiferromagnetic state at $x>0.5$. At $x \sim 0.5$, where both the T_C and T_N become comparable, the charge or orbital ordering appears.

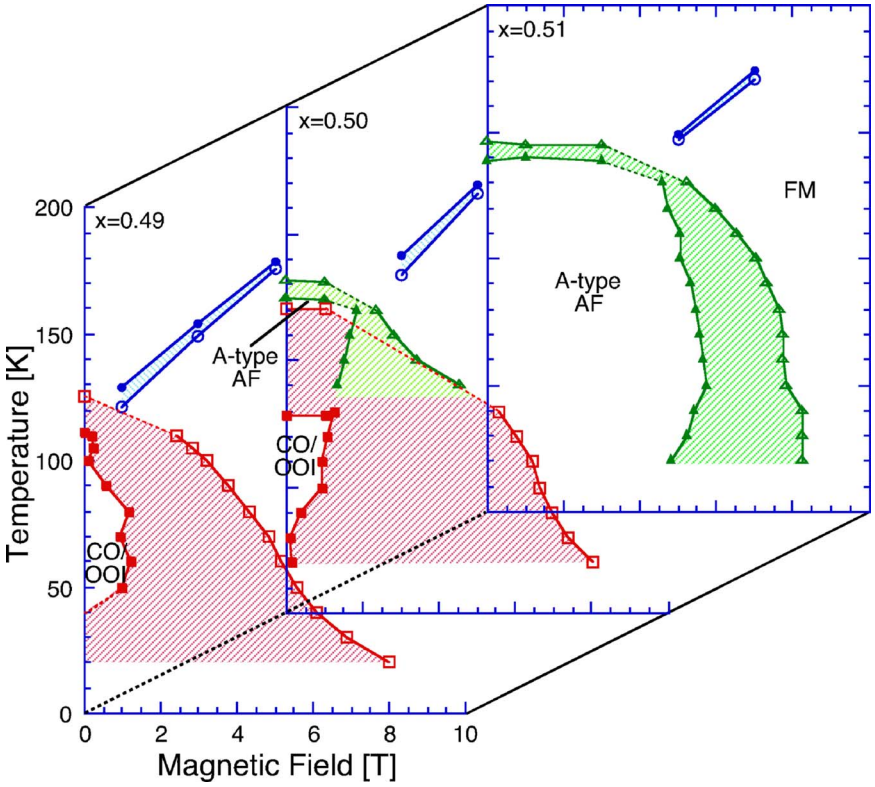

FIG. 6. (Color online) The phase diagrams among the CO/OOI, the *A*-type antiferromagnetic nonmetal and the FM for the $Sm_{1-x}Sr_xMnO_3$ with $x=0.49$, 50, and 0.51 crystals, which are plotted on the temperature versus the magnetic field plane. The transitions from (to) the CO/OOI are denoted as open (solid) squares, and those from (to) the *A*-type antiferromagnetic nonmetal are open (solid) squares, respectively. The temperatures for the metal-insulator transitions defined in the temperature profiles of resistivity are denoted as open (cooling runs) and closed (warming) circles, respectively. The hystereses are hatched.

At $x=0.5$, the crystal first undergoes the transition to the *A*-type antiferromagnetic state at ~130 K and subsequently to the *CE*-type antiferromagnetic charge or orbital-ordered state at ~80 K as temperature decreases. The point of ($x \sim 0.5$, $T \sim 120$ K) on the electronic phase diagram (the critical temperatures versus the x plane) is thus considered as a multicritical point. As the compound approaches this multicritical point from the higher temperature side, the fluctuations, or the short-range correlations of the *A*-type antiferromagnetism and the charge or orbital ordering are both observed in x-ray and/or neutron scattering as the competitors with the ferromagnetic state.

We have also studied the field-induced phenomena for the crystals around $x=0.5$. At $x=0.49$, the ferromagnetic metal and the charge or orbital-ordered insulator coexist. The charge or orbital-ordered insulator as the ground state at $x=0.5$ changes to the *A*-type antiferromagnetic nonmetal at $x=0.51$. For the $x=0.49$, 0.50, and 0.51 crystals, we have demonstrated also on the temperature versus magnetic-field plane the multicritical phase competition among the charge or orbital-ordered insulator, the *A*-type antiferromagnetic nonmetal, and the ferromagnetic metal.

ACKNOWLEDGMENT

The authors would like to thank R. Kumai for his help in x-ray diffraction experiments.

[1] Y. Tokura, Rep. Prog. Phys. **69**, 797 (2006).
[2] J. B. Torrance, P. Lacorre, A. I. Nazzal, E. J. Ansaldo, and Ch. Niedermayer, Phys. Rev. B **45**, 8209 (1992).
[3] C. Zener, Phys. Rev. **82**, 403 (1951).
[4] P. W. Anderson and H. Hasegawa, Phys. Rev. **100**, 675 (1955).
[5] P.-G. de Gennes, Phys. Rev. **118**, 141 (1960).
[6] Y. Tokura, A. Urushihara, Y. Moritomo, T. Arima, A. Asamitsu, G. Kido, and N. Furukawa, J. Phys. Soc. Jpn. **63**, 3931 (1994).
[7] A. Urushibara, Y. Moritomo, T. Arima, A. Asamitsu, G. Kido, and Y. Tokura, Phys. Rev. B **51**, 14103 (1995).
[8] H. Kuwahara, Y. Tomioka, A. Asamitsu, Y. Moritomo, and Y. Tokura, Science **270**, 961 (1995).
[9] H. Kuwahara, Mater. Res. Soc. Symp. Proc. **494**, 83 (1998).
[10] R. Kajimoto, H. Yoshizawa, H. Kawano, H. Kuwahara, Y. Tokura, K. Ohoyama, and M. Ohashi, Phys. Rev. B **60**, 9506 (1999).
[11] R. Maezono, S. Ishihara, and N. Nagaosa, Phys. Rev. B **57**, R13993 (1998).
[12] R. Maezono, S. Ishihara, and N. Nagaosa, Phys. Rev. B **58**, 11583 (1998).
[13] C. Martin, A. Maignan, M. Hervieu, and B. Raveau, Phys. Rev. B **60**, 12191 (1999).
[14] V. Yu. Ivanov, A. A. Mukhin, V. D. Travkin, A. S. Prokhorov, and A. M. Balbashov, J. Magn. Magn. Mater. **258–259**, 535 (2003).
[15] V. Yu. Ivanov, A. A. Mukhin, A. S. Prokhorov, and A. M. Balbashov, Phys. Status Solidi A **236**, 445 (2003).
[16] F. Damay, C. Martin, M. Hervieu, and B. Raveau, Solid State Commun. **98**, 997 (1996).
[17] A. I. Kurbakov, A. V. Lazuta, V. A. Ryzhov, V. A. Trounov, I. I.

Larionov, C. Martin, A. Maignan, and M. Hervieu, Phys. Rev. B **72**, 184432 (2005).
[18] N. A. Babushkina, E. A. Chistotina, O. Yu. Gorbenko, A. R. Kaul, D. I. Khomskii, and K. I. Kugel, Phys. Rev. B **67**, 100410(R) (2003).
[19] N. A. Babushkina, E. A. Chistotina, O. Yu. Gorbenko, A. R. Kaul, D. I. Khomskii, and K. I. Kugel, J. Magn. Magn. Mater. **272–276**, 407 (2004).
[20] N. A. Babushkina, E. A. Chistotina, O. Yu. Gorbenko, A. R. Kaul, K. I. Kugel, A. I. Kurbakov, V. A. Trunov, and J. Andre, Phys. Solid State **46**, 1884 (2004).
[21] L. M. Fisher, A. V. Kalinov, I. F. Voloshin, N. A. Babushkina, D. I. Khomskii, Y. Zhang, and T. T. M. Palstra, Phys. Rev. B **70**, 212411 (2004).
[22] M. Uehara, S. Mori, C. H. Chen, and S.-W. Cheong, Nature (London) **399**, 560 (1999).
[23] A. Moreo, M. Mayr, A. Feiguin, S. Yunoki, and E. Dagotto, Phys. Rev. Lett. **84**, 5568 (2000).
[24] J. Burgy, M. Mayr, V. Martin-Mayor, A. Moreo, and E. Dagotto, Phys. Rev. Lett. **87**, 277202 (2001).
[25] E. Dagotto, T. Hotta, and A. Moreo, Phys. Rep. **344**, 1 (2001).
[26] Y. Motome, N. Furukawa, and N. Nagaosa, Phys. Rev. Lett. **91**, 167204 (2003).
[27] L. M. Rodriguez-Martinez and J. P. Attfield, Phys. Rev. B **54**, R15622 (1996).
[28] L. M. Rodriguez-Martinez and J. P. Attfield, Phys. Rev. B **63**, 024424 (2000).
[29] Y. Tomioka and Y. Tokura, Phys. Rev. B **70**, 014432 (2004).
[30] Y. Endoh, H. Hiraka, Y. Tomioka, Y. Tokura, N. Nagaosa, and T. Fujiwara, Phys. Rev. Lett. **94**, 017206 (2005).
[31] Y. Tomioka, Y. Okimoto, J. H. Jung, R. Kumai, and Y. Tokura, Phys. Rev. B **68**, 094417 (2003).
[32] S. Shimomura, N. Wakabayashi, H. Kuwahara, and Y. Tokura, Phys. Rev. Lett. **83**, 4389 (1999).
[33] S. Shimomura, T. Tonegawa, K. Tajima, N. Wakabayashi, N. Ikeda, T. Shobu, Y. Noda, Y. Tomioka, and Y. Tokura, Phys. Rev. B **62**, 3875 (2000).
[34] H. Kuwahara, T. Okuda, Y. Tomioka, A. Asamitsu, and Y. Tokura, Phys. Rev. Lett. **82**, 4316 (1999).